

Aerodynamic sound of turbulent time-developing shear layer as the outcome of the flow linear non-modal instability

George Khujadze^{a,1} David Gogichaishvili,² George Chagelishvili,^{3,4}
Alexander Tevzadze,^{3,5} Jan-Niklas Hau,⁶ and Holger Foysi¹

¹*Chair of Fluid Mechanics, Universität Siegen, 57068 Siegen, Germany*

²*Department of Physics, The University of Texas at Austin, Austin 78712, USA*

³*E. Kharadze Georgian National Astrophysical Observatory, Abastumani 0301, Georgia*

⁴*Institute of Geophysics, Tbilisi State University, Tbilisi 0128, Georgia*

⁵*Kutaisi International University, Kutaisi 4600, Georgia*

⁶*Technische Universität Darmstadt, Darmstadt, 64287, Germany^b*

(Dated: April 21, 2021)

The aim of this paper is to substantiate the importance of non-normality of shear flow linear operators and its consequence – the non-modal dynamics of the perturbations – in the formation of acoustic wave output of time-developing free shear/mixing layers. Initially, the linear transient dynamics of spatial Fourier harmonics is considered in a 3D homentropic parallel unbounded inviscid constant shear flow which can model the central/body part of the shear layer. The non-modal approach allows to capture the only linear mechanism of the acoustic wave generation – *the linear vortex-wave mode coupling induced by the shear flow non-normality*. We describe the specific/key features of the generation process that should leave traces on the further dynamics of the generated waves. Thereafter, the results of direct numerical simulations of compressible turbulent time-developing mixing layers for a moderate convective Mach number (specifically, $M_c = 0.7$) and simulation boxes (L_x, L_y, L_z) with fixed streamwise and shearwise lengths ($L_x = 100, L_y = 200$) and different streamwise-spanwise aspect ratios ($L_x/L_z = 0.5, 1, 2$) are presented. The simulations identify the origin of the acoustic wave output: the dominance of a *linear generation process of acoustic waves in the shear layer core region, induced by the flow non-normality*, observable in the near field of acoustic waves emitted by the flow.

The non-modal physics of the perturbation dynamics studied here, utilizing the example of a time developing compressible turbulent mixing layer, must be essential also for other turbulent engineering shear flows as the non-normality is their inherent feature. This will be relevant also for engineering compressible shear flows with exponentially growing “modal solutions”, whose finite time period dynamics/growth undergoes a significant change due to the non-modal physics. The consideration of the non-modal effects (that has been successfully adopted in hydrodynamic, atmospheric and astrophysical flow communities since the 1990s) is necessary in order to properly describe the flow’s real dynamics and, most importantly in the context of our study, to get physical insight into the formation of the near acoustic field.

I. INTRODUCTION

Aerodynamic sound generation is a major subject of fluid dynamics research and represents an enormous scientific and technological challenge. A simplified model to get physical insight into the mechanisms of aerodynamic sound generation in jets and other turbulent flows is the compressible free shear or mixing layer – the flow consisting of two parallel streams of fluid with unequal velocities – as it mimics shear layer regions of some natural and engineering nonuniform flows. For quite some time already it became clear that the flow turbulence is a mix of chaotic and coherent motions, focusing interest on coherent structures in search of aerodynamic sound sources. According to the formed view, the main sources of the aerodynamic sound emitting from shear layers are large-scale structures in the form of wave-packets – perturbative structures that are spatio-temporally coherent over distances and times usually larger than the integral scales of the turbulence. The dominance of these wave-packet-type sources of sound for supersonic shear layers was shown in [1]. In the case of subsonic shear layers, there are strong experimental, theoretical and computational evidences of the wave-packets effectiveness as the source of most of the sound output (see, e.g., [2–5]). The importance of wave-packets in acoustics can be learned from [6], where their existence, energetics, dynamics and acoustic efficiency for jet flow configurations is exhaustively reviewed. On the basis of the extensive number of simulations and modern measurement techniques discussed in there, wave-packets are represented “as instability waves, or more general *modal solutions* of the governing equations”, confirming their acoustic importance in high subsonic and supersonic jets. Highlighting the phrase “modal solution” by us is intentional, as this concept is the

^a Corresponding author: george.khujadze@uni-siegen.de

^b The main contribution of this author happened when still at Darmstadt Technical university. *Present address:* Frankfurt, Germany

turning point of our analysis. Specifically, it turned out that the traditional modal analysis of the perturbation dynamics in shear flows is not optimal and can be misleading in many respects.

Shortcomings of the traditional modal analysis of linear processes in shear flows (the spectral expansion of perturbations in time with subsequent analysis of its eigenmodes) were rigorously revealed by the hydrodynamic community in the 1990s (see, e.g., [7–13]).

Operators with nonorthogonal eigenfunctions are referred to as non-normal [14, 15]. Consequently, flows with such operators are referred to as non-normal. It has been shown that the operators of the modal analysis of linear processes in shear flows are exponentially far from normal [12, 13, 16] (the norm of the flow non-normality increases with the shear rate). Due to this non-normality, the eigenmodes strongly interfere and a suitable approach needs to be applied in order to fully analyze this behavior - the analysis of eigenmodes, treated as linearly independent, is misleading. In the framework of the classical modal approach, that focuses on the asymptotic stability of flows, little attention is paid to any particular initial value or finite time period of the dynamics. Consequently, the transient behavior, that is the characteristic feature of the dynamics of shear flows, is considered as non-significant. By discarding the modal analysis and adopting the so-called non-modal approach to aerodynamic sound generation, manifestations of the flow non-normality can be traced in the acoustic wave output of, for instances, time-developing mixing layers (with streamwise and spanwise periodic boundary conditions). The non-modal approach reveals a remarkably rich picture of the linear perturbation behavior – e.g., vortex–wave mode coupling – that greatly differs from solutions of the modal approach. Mathematically, the linear vortex–wave mode coupling has been rigorously studied. Taking the specifics of the linear coupling into account, numerous examples of spontaneous wave generation by vortex mode disturbances in atmospheric, astrophysical and magnetized smooth shear flows are already studied and described in detail [17–27]. As for the acoustic wave generation, the coupling has been analyzed numerically for mode-dependent moderate and large Mach numbers [28–31], as well as in terms of Stokes lines for small Mach numbers [32].

Here, the following should also be emphasized. Generally, the shear flow non-normality essentially changes the finite time period of the dynamics. This concerns not only the appearance of the new type of linear transient phenomenon, the vortex–wave mode coupling, but also relates to exponentially growing “modal solutions”, whose initial, finite time period dynamics/growth undergoes a significant change. It is necessary to take into account the non-modal effects on the exponentially growing mode dynamics instead of relying solely on its modal growth, in order to properly describe their real dynamics. This view about the importance of non-modal physics in the dynamics of exponentially growing modes is well comprehended by the astrophysical disks community [33, 34]. Astrophysical disks are highly non-normal sheared flows due to their strong differential rotation. Consequently, the flow non-normality is investigated in all its manifestations and one can use the experience and knowledge of the astrophysical disk community for the investigation of the sound production in engineering turbulent shear flows. One example of the necessity of making use of this description can be given. The modal approach describes exponentially/spectrally unstable modes of wave-packets in jet flows [6]. This description can be misleading, however, without involving the flow non-normality modifications of the spectrally unstable mode dynamics.

In this paper we consider the compressible mixing layer, a simplified, and thus, convenient model to provide physical insight into the mechanisms of aerodynamic sound generation in jet and other turbulent engineering flows. This flow mimics shear layer regions of jets and, furthermore, by itself, occurs in many natural and engineering flows, being therefore just sophisticated enough to observe the relevant physics of interest, here. The object of our study is the time-developing mixing layer, because the numerically simulated fully nonlinear/turbulent dynamics of this flow enables us to follow quite clearly the outcomes of the vortex–wave linear coupling in smooth shear flows. Indeed, the central/core part of the time-developing mixing layer (i.e. the area between the near boundary/turning areas) can be modeled as a constant shear flow. This central part of the flow is energetically active due to the non-normality: this ensures linear transient growth of certain Fourier harmonics of vortex mode perturbations and linear generation of acoustic wave harmonics by related vortex mode ones. The boundary areas modify the dynamics of the central part in a certain way. However, the latter still enables to grasp the phenomena that appear in linearly sheared regions and can therefore form the basis of far-field sound of more complex nonuniform flows.

First of all, we investigate the linear generation of acoustic waves by vortex modes in a 3D homentropic parallel unbounded inviscid constant shear flow: $\mathbf{U}_0 = (Ay, 0, 0)$, where the flow is directed along the x -axis, the flow shear with parameter A – along y axis. We consider the dynamics of a single pure vortex mode Fourier harmonic $(k_x, k_y(t), k_z)$. According to the non-modal approach the shearwise wavenumber of harmonics depends linearly on time, $k_y(t) = k_y(0) - Ak_x t$. The linear generation of acoustic waves and its characteristics are grasped by studying initially highly up-shear tilted pure vortex mode Fourier harmonics, $k_y(0)/k_x \gg 1$, independent of the value of the spanwise wavenumber, k_z . The generation process of the acoustic wave harmonics is specific and occurs due to linear transient vortex–wave mode coupling, induced by the shear flow non-normality. While the potential vorticity of the imposed vortex mode harmonic is preserved in time, a wave part appears just when the time-dependent shearwise wavenumber of the analyzed harmonic becomes zero. The key to comprehending the mathematical aspect of the wave generation is rooted in the possibility of splitting the velocity field of the considered harmonic into its vortex and wave

parts at exactly this time. The potential vorticity of the harmonic is fully contained in the vortex part, which evolves aperiodically when tilted down-shear ($k_y/k_x < 0$). At the same time, the down-shear tilted wave part has a zero potential vorticity and exhibits an oscillating nature in time. The performed analysis reveals the key characteristics of acoustic wave harmonics' generation process: increase of the efficiency of the wave generation with the increase of streamwise length scale of the vortex harmonics; abrupt emergence of the wave harmonics from the vortex ones; regular/fixed phase of the wave harmonics at the moment of emergence (that is the basis of constructive interference of the linearly generated harmonics). These key characteristics are due to the specific nature of the linear vortex–wave mode coupling induced by shear flow non-normality.

Next we perform direct numerical simulations (DNS) of compressible turbulent time-developing mixing layers for moderate convective Mach number, $M_c = 0.7$, and simulation boxes, (L_x, L_y, L_z) , for fixed streamwise and shearwise lengths ($L_x = 100, L_y = 200$) and different streamwise-spanwise aspect ratios ($L_x/L_z = 0.5, 1, 2$). The size of the computational boxes in the shear direction, L_y , exceeds the shear layer thickness a few times, allowing to grasp the acoustic wave output (*near wave field*) of the layer and its characteristics. The choice of the convective Mach number and the streamwise and spanwise lengths of the boxes mainly make the harmonics with the largest streamwise wavelength “acoustically active”, ensuring the identification of the origin of the near wave field, emitted mostly because of the only linear mechanism of the acoustic wave generation in the central part of the flow induced by its non-normality [35]. The dominance of this linear mechanism in the aerodynamic sound generation points out the shortcomings of the traditional modal analysis of linear processes in shear flows. The proposed view is in accordance with the established picture about the decisive role of large-scale structures in shear layers (i.e. wave-packets) in aerodynamic sound radiation. However, it diverges with it by the features of the linear generation of acoustic waves: shear flows are nonnormal and the generation analysis in the framework of the modal approach is misleading unless analyzed in the framework of the non-modal approach. The basic/simplest “elements” of aerodynamic sound generation are considered not entire and undivided wave packets, but their “building blocks”: vortex mode Fourier harmonics, or, differently, Kelvin modes.

The Numerical simulations in this paper show a mostly 2D regular character of the acoustic wave field output at $L_x/L_z = 2$; the appearance of slight 3D features of the output at $L_x/L_z = 1$ and a further significant increase of the output irregularity at $L_x/L_z = 0.5$, that forms complex (almost chaotic) picture containing a significant 3D component of the near acoustic field. In reality, all these are in exact accordance with the above mentioned linear transient vortex–wave mode coupling induced by the shear flow non-normality.

The structure of the paper is as follows: In section II we outline the linear generation of acoustic waves by vortex modes in the constant shear flow focusing on key features (abrupt and regular character) of the emergence of acoustic wave harmonics from the vortex ones and on the dependence of the wave generation efficiency on the ratio k_z/k_x . In section III the results of DNS of turbulent time-developing shear layer are presented and the acoustic wave field output of the shear layer is analyzed to show the decisive role of the linear aerodynamic sound generation induced by the flow non-normality in the forming of the far-field. Summary and discussions are given in section IV.

II. THE LINEAR GENERATION OF ACOUSTIC WAVES BY VORTEX MODES IN CONSTANT SHEAR FLOWS

The central region of time-developing mixing layer can be modeled by constant shear flow that is energetically active due to the non-normality: it ensures a linear transient growth of certain harmonics of the vortex mode perturbations and the linear generation of acoustic wave harmonics by related vortex modes [28–31]. Of course, dynamical processes in the central region of the shear layer are influenced, in reality, by the processes in the boundary areas of the flow. However, the linear transient processes can give birth to acoustic waves in the central region (approximated by constant shear), which form the significant (even dominant) portion of the near wave field of the flow.

Here, we outline the essence of the acoustic wave linear generation process in 2D and 3D parallel inviscid constant shear flow, with uniform density and pressure, $U_0(Ay, 0, 0)$, ρ_0 , $P_0 = \rho_0 c_s^2$, respectively, with c_s being the speed of sound. Employing the standard method of the non-modal approach the spatial Fourier harmonics of perturbations with a time-dependent shear-wise wavenumber, $k_y(t)$, are introduced [28, 31]:

$$\Psi(x, y, z, t) = \Psi(k_x, k_y(t), k_z, t) e^{ik_x x + k_y(t)y + k_z z},$$

where $k_y(t) = k_y(0) - k_x A t$. $\Psi \equiv (u_x, u_y, u_z, \rho, p)$ denotes the velocity components, density and pressure of spatial Fourier harmonics, respectively. In physical space (x, y, z) , the above representation describes a harmonic plane wave – so-called, Kelvin mode – with time-dependent amplitude and shearwise wavenumber. The variation of $k_y(t)$ is caused by the shearing of the harmonics due to the background flow.

The physical variables are normalized as follows

$$\begin{aligned} \mathbf{v} &= \frac{\mathbf{u}}{c_s}, \quad D = i \frac{\rho}{\rho_0} = i \frac{p}{P_0}, \quad \tau = c_s k_x t, \quad \mathcal{M} = \frac{A}{k_x c_s}, \\ \gamma &= \frac{k_z}{k_x}, \quad \beta(\tau) = \frac{k_y(0)}{k_x} - \mathcal{M}\tau = \beta(0) - \mathcal{M}\tau, \end{aligned} \quad (1)$$

where \mathcal{M} is the normalized shear rate and characterizes compressibility of the 2D harmonics with streamwise wavenumber k_x . We call \mathcal{M} the mode-dependent Mach number of a 2D harmonic.

3D harmonics have a different measure of compressibility. Therefore, we separately introduce the mode-dependent Mach number at an arbitrary moment of time, $\mathcal{M}_D(\tau)$, as the ratio of the normalized shear rate, \mathcal{M} , to the normalized instant frequency of the harmonic, $\omega(\tau) = \sqrt{1 + \beta^2(\tau) + \gamma^2}$:

$$\mathcal{M}_D(\tau) \equiv \frac{\mathcal{M}}{\omega(\tau)} = \frac{\mathcal{M}}{\sqrt{1 + \beta^2(\tau) + \gamma^2}} \quad (2)$$

The maximum of \mathcal{M}_D is reached at the critical time $\tau^* = \beta(0)/\mathcal{M}$, i.e., at the moment the Fourier harmonics cross the k_x -axis (the line $k_y = 0$). At this point the measure of compressibility of a 3D mode reaches its maximum, defined as:

$$\mathcal{M}^* \equiv \max(\mathcal{M}_D(\tau)) = \frac{\mathcal{M}}{\sqrt{1 + \gamma^2}} \quad (3)$$

This mode-dependent Mach number determines the linear mode-coupling for the related 3D harmonic and, consequently, the efficiency of the wave generation. The above equation shows that \mathcal{M}^* has a maximum for the 2D harmonics (when $\gamma = 0$) and decreases with increase of γ , consequently, the wave generation should be maximal for 2D harmonics and should decrease with an increase of γ . These facts are confirmed by the calculations below.

At $\beta(0) \gg 1$, when $\mathcal{M}_D \ll 1$, the compressibility characteristics of the harmonic substantially diminishes and the separation between acoustic waves and vortex motion becomes possible. Hence, we determine vortex mode harmonics in these regions similar to [31] in order to study the generation of oscillating and propagating wave mode perturbations by initially pure (void of wave modes) vortex modes. By extracting the vortex part in regions of $\beta(0) \gg 1$ and subsequently exploiting the properties of vortex modes, one can find harmonics of pure vortex perturbations in any region/point of the wavenumber space.

The considered constant shear flow system contains an essential, temporally conserved parameter for each harmonic called the potential vorticity

$$\mathcal{W} = (1 + \gamma^2) v_y - \beta(\tau)(v_x + \gamma v_z) - \mathcal{M}D. \quad (4)$$

The vortex mode harmonics has non-zero potential vorticity and zero group velocity, whereas the acoustic wave mode harmonics give rise to zero potential vorticity and non-zero group velocity. By initially imposing highly up-shear tilted pure vortex mode harmonics ($\beta(0) \gg 1$) in the linearized equations, the emergence of the acoustic wave harmonics by the linear vortex-wave mode coupling caused by the shear flow non-normality was investigated in [28, 31]. The efficiency of this mechanism depends on *the harmonic's (mode-dependent) Mach number*. The wave generation for 2D harmonics is noticeable at $\mathcal{M} = 0.2$ and substantial already at $\mathcal{M} > 0.3$. We would like to emphasize that we operate in terms of two different definitions of Mach numbers: a *mode-dependent Mach number* (\mathcal{M} for 2D harmonics and \mathcal{M}^* for the 3D case) and a *convective Mach number* (M_c). The first definition is related to separate Fourier harmonics of perturbations and the second determines the flow compressibility effects in general (in our case that of a time-developing mixing layer).

The plots in the left column in Figure 1 show the dynamics of v_x , v_y , v_z and D at $\mathcal{M} = 0.4$, $\beta(0) = 10$, $\gamma = 0, 0.5, 1$. The black, red and blue curves represent time evolution of harmonics with $\gamma = 0, 0.5, 1$, respectively. The imposed vortex mode harmonic remains aperiodic up to $\tau < \beta(0)/\mathcal{M} \equiv \tau^* = 25$, i.e., at $\beta(\tau) > 0$. The oscillating/wave nature appears just at $\tau > \tau^*$, i.e., at $\beta(\tau) < 0$. The shear-wise wave number of the harmonics, $\beta(\tau)$ (or $k_y(t)$ in dimensional units), is time dependent. One can say, that the harmonics “drift” in spectral space along the k_y axis and each wave harmonic emerges from the related vortex one when crossing of the k_x axis (or $k_y = 0$ line) during this “drift”, that occurs at the critical time τ^* that is a universal timescale for the appearance of linearly generated waves.

This peculiar behavior motivates the introduction of a numerical mode-splitting at $\tau = \tau^*$, in spite of the strong vortex-wave mode coupling in the its vicinity [28]. Although the wave and vortex mode parts are not distinguishable at $|\beta(\tau)| < 1$, the mathematical separation is useful as it allows to understand the different behavior of the vortex and wave mode harmonics during their further dynamics. It is possible to extract a vortex mode harmonic at $\tau = \tau^*_+$

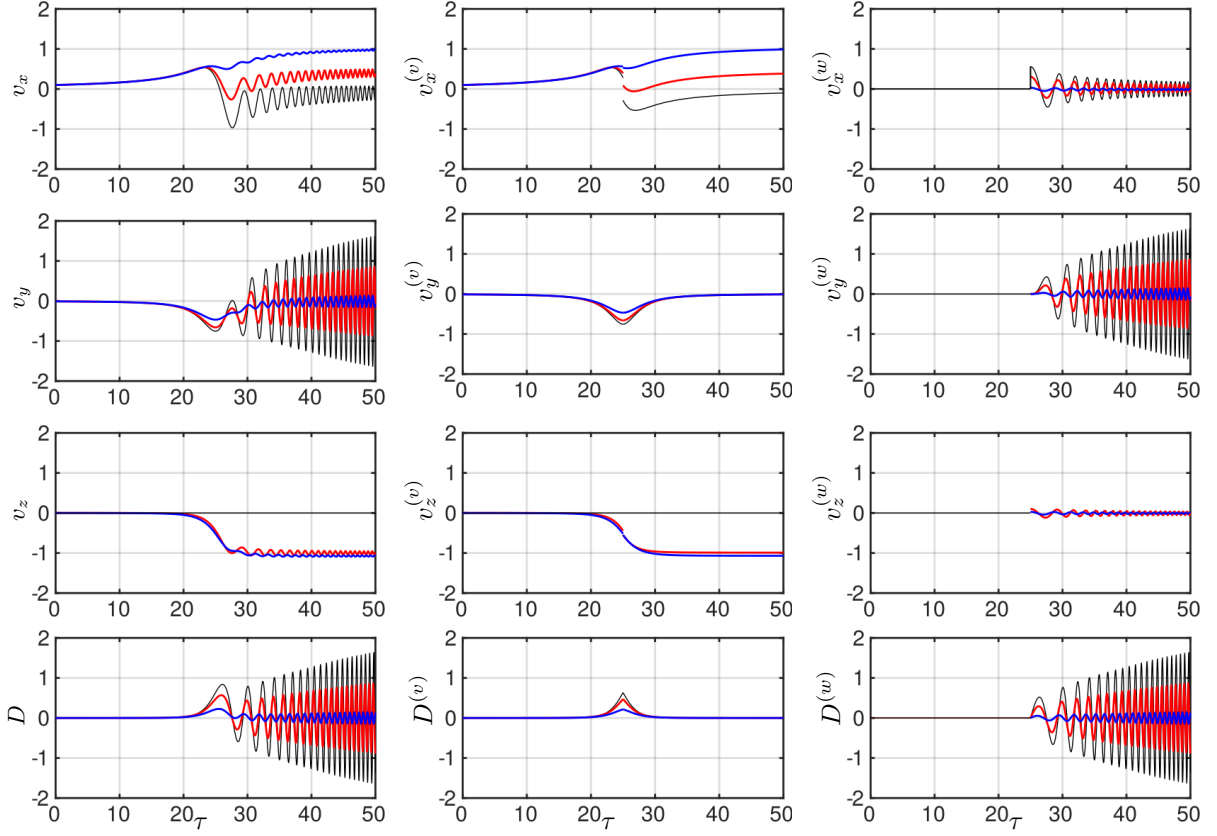


FIG. 1: The dynamics of (v_x, v_y, v_z, D) (left column) and their vortex (v) (central column) and wave (w) (right column) parts for the initially pure vortex harmonic $(v_x^{(w)}(0), v_y^{(w)}(0), v_z^{(w)}(0), D^{(w)}(0) = 0)$ for $\mathcal{M} = 0.4$, $\beta(0) = 10$ and $\gamma = 0, 0.5, 1$. Black, red and blue lines correspond to 2D ($\gamma = 0$), 3D ($\gamma = 0.5$) and ($\gamma = 1$) cases, respectively. For the considered Mach number the wave generation is maximal for 2D case. For $\gamma = 0.5$ case, the wave generation is somewhat reduced compared to $\gamma = 0$ case. For $\gamma = 1$ case, the wave generation is substantially reduced (almost negligible) compared to $\gamma = 0$ case.

(where $\tau_{\pm}^* \equiv \tau^* \pm 0$), that further evolves independently of the wave mode harmonic and retains its aperiodic nature. We can therefore split the velocity and density perturbations as

$$\begin{aligned}
 v_x(\tau_-^*) &\equiv v_x^{(v)}(\tau_-^*) = v_x^{(v)}(\tau_+^*) + v_x^{(w)}(\tau_+^*), \\
 v_y(\tau_-^*) &\equiv v_y^{(v)}(\tau_-^*) = v_y^{(v)}(\tau_+^*) + v_y^{(w)}(\tau_+^*), \\
 v_z(\tau_-^*) &\equiv v_z^{(v)}(\tau_-^*) = v_z^{(v)}(\tau_+^*) + v_z^{(w)}(\tau_+^*), \\
 D(\tau_-^*) &\equiv D^{(v)}(\tau_-^*) = D^{(v)}(\tau_+^*) + D^{(w)}(\tau_+^*),
 \end{aligned}$$

where the superscripts (v) and (w) denote the vortex and wave parts, respectively. The plots in the central column of Figure 1 show the dynamics of the vortex part of the related quantities whereas the plots in the right column show the dynamics of the wave part. To summarize the results of the splitting:

- (i) There is an abrupt emergence of an acoustic wave harmonic from the vortex one at the crossing of the k_x -axis during the “drift”;
- (ii) The generation mechanism is anisotropic – the generated acoustic wave harmonics can be found only in those parts of spectral space where $k_y/k_x \leq 0$;
- (iii) The gap in the evolution of the vortical part of the streamwise velocity perturbation, $v_x^{(v)}(\tau_+^*) - v_x^{(v)}(\tau_-^*)$, is a measure of the spontaneously generated wave harmonic;
- (iv) The wave harmonics emerge abruptly with very regular phase. At the moment of the emergence the shearwise velocity and density of the wave harmonic ($v_y^{(w)}(\tau_+^*), D^{(w)}(\tau_+^*) = 0$) are zero, while the values of the streamwise and spanwise velocities ($v_x^{(w)}(\tau_+^*), v_z^{(w)}(\tau_+^*)$) are maximal;

(v) The mutual Independence of the dynamics of the vortex and wave parts of the quantities occurs for $\tau > \tau^*$ indicating the validity of the splitting at $\tau = \tau^*$;

(vi) For the considered mode-dependent Mach number, $\mathcal{M} = 0.4$, the generation of 2D wave harmonics prevails over 3D ones – the generation of 3D wave harmonics decreases rapidly with increasing $\gamma = k_z/k_x$.

We should note additionally, that the topology of the summarized anisotropic linear generation mechanism differs principally from the topology of the linear source representations in the classical formulations of the acoustic analogy [31]. The linear source terms of the latter are distributed in all regions/quadrants of the spectral space ($k_y/k_x > 0$ and $k_y/k_x < 0$) predicting the immediate emergence of wave harmonics in any of the quadrants. This makes acoustic analogies incompatible with the linear mechanism of generation of wave harmonics by vortex mode harmonics in shear flows, induced by the non-normality.

According to the literature, an entire wave-packet is the source of the acoustic wave generation and the latter process is described in the framework of the modal/spectral approach. However, in fact, wave-packets are composed of coherent vortex mode harmonics that represent the basic “elements” of dynamic processes under linear shear [36]. There is an abrupt emergence of waves from the initial vortex mode at $\tau = \tau^*$ with the amplitude of streamwise and spanwise velocities, $v_x^{(w)}(\tau^*) = v_x^{(v)}(\tau_-^*) - v_x^{(v)}(\tau_+^*)$ and $v_z^{(w)}(\tau^*) = v_z^{(v)}(\tau_-^*) - v_z^{(v)}(\tau_+^*)$. Consequently, the basic process is the linear generation of acoustic wave harmonics by the related vortex modes. Therefore, the basic source of acoustic waves are vortex mode harmonics and not an entire/undivided wave-packet – the packet just collects via constructive interference the acoustic wave harmonics generated by the basic process.

Efficacy of the wave generation

The efficacy of the wave generation process is identified by the jump occurring in the vortex part of the dependent (split) variables ($v_x^{(v)}$, $v_y^{(v)}$, $v_z^{(v)}$, $D^{(v)}$) at $\tau = \tau^*$ and the thereby generated wave harmonic [37, 38]. This is directly seen in Figure 1 for the streamwise and spanwise perturbation velocities. Although not visible, the jump naturally occurs in the derivatives of the remaining quantities. Thus, we define the efficacy of the wave generation process by initially pure vortex mode perturbations as the ratio of the wave energy to the vortex one

$$\eta \equiv \frac{E^{(w)}(\tau_+^*)}{E^{(v)}(\tau_-^*)} = \frac{|v_x^{(w)}(\tau_+^*)|^2 + |v_z^{(w)}(\tau_+^*)|^2}{|v_x^{(v)}(\tau_-^*)|^2 + |v_y^{(v)}(\tau_-^*)|^2 + |v_z^{(v)}(\tau_-^*)|^2 + |D^{(v)}(\tau_-^*)|^2}, \quad (5)$$

where the fact that $|v_y^{(w)}(\tau_+^*)|^2 = 0$ and $|D^{(w)}(\tau_+^*)|^2 = 0$ is taken into account.

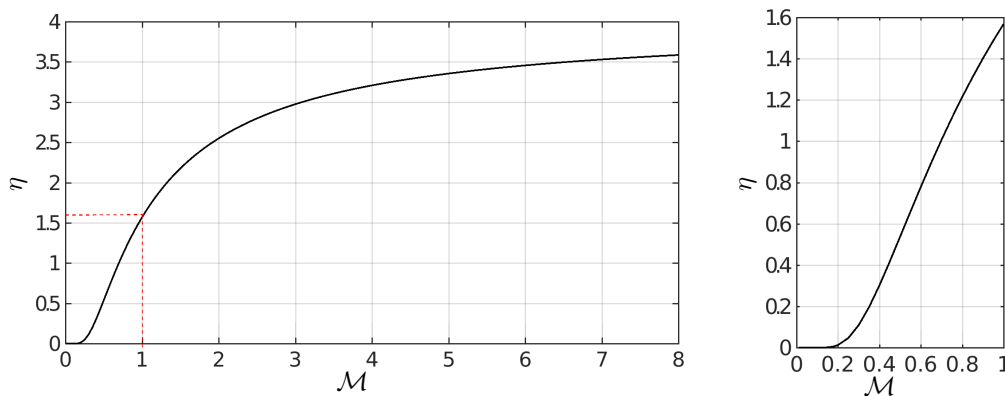


FIG. 2: The dependence of the effective parameter of linear generation of acoustic wave harmonics by related vortex mode ones, η , on \mathcal{M} for the 2D case (i.e., at $\gamma = 0$) for $\beta(0) = k_y(0)/k_x = 10$. The left plot is for a wide range of Mach number values, while the right plot shows the zoomed view of η for $\mathcal{M} \in [0, 1]$.

In Figure 2 the dependence of the effective parameter of wave generation, η , on \mathcal{M} for the 2D case (i.e., at $\gamma = 0$) is presented. The left plot is for a wide range of Mach number values, while the right one shows a zoomed view of η for the region $\mathcal{M} \in [0, 1]$. The process of the wave generation becomes noticeable at $\mathcal{M} = 0.2$ and substantial already at $\mathcal{M} = 0.3$. The growth of η becomes gentle from $\mathcal{M} = 2$ and asymptotically tends to 4 at $\mathcal{M} \rightarrow \infty$. The right plot clearly shows a sharp change of η for a moderate $\mathcal{M} \in [0.3, 1]$. We operate in the range of $\mathcal{M} \in [0.1, 1]$ mode-dependent Mach numbers to establish the importance of the discussed linear mechanism of wave generation in

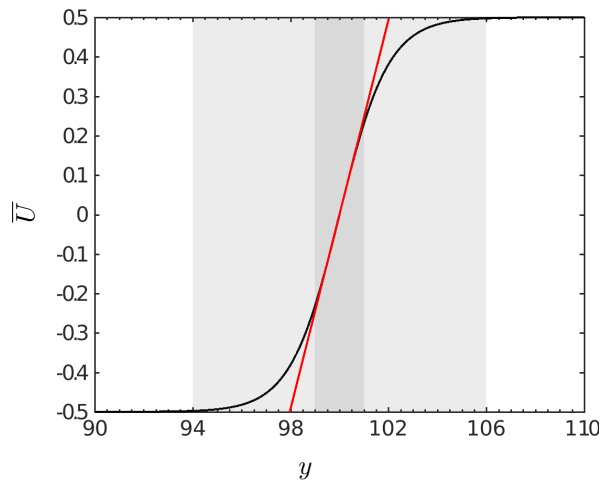


FIG. 3: Mean velocity profile at initial moment of time. The red line shows the maximum gradient of the mean velocity profile. One can consider the grey area as the shear layer area (where the mean velocity gradient is non-zero). The dark grey area represents the central/body/core region of the flow with linear profile of mean velocity which matches to the red line.

the case of a compressible turbulent time-developing mixing layer, the results of that numerical study is presented in the next section. One has to note, that η is not the efficiency of the wave generation itself, since it reaches values larger than one. This indicates that the wave energy growth is provided by the flow shear, while vortex disturbances only trigger/mediate the generation process.

Equation (5) for the 3D case has to be evaluated numerically, as the jump occurring around $\tau = \tau^*$ does not follow an exact analytical relation contrary to the 2D case. Hereby, we fix the initial wavenumber ratio $\beta(0) = k_y(0)/k_x = 10$, while varying the perturbation Mach number \mathcal{M} and the wavenumber ratio $\gamma = k_z/k_x$. From figure 2 it follows that the efficacy of the wave generation, specifically, for $\mathcal{M} = 0.4$ and 2D harmonics is $\eta(\mathcal{M} = 0.4, \gamma = 0) = 0.32$. The calculations show that the efficacy decreases with γ : $\eta(\mathcal{M} = 0.4, \gamma = 0.5) = 0.15$, $\eta(\mathcal{M} = 0.4, \gamma = 1) = 0.0022$ and $\eta(\mathcal{M} = 0.4, \gamma = 2) = 3.2 \cdot 10^{-7}$, etc.

Generally, the efficacy of the linear mechanism of wave generation by a pure vortex mode harmonic for moderate mode-dependent Mach numbers, $\mathcal{M} \lesssim 1$, reaches maximum for 2D harmonics and decreases quite fast with an increase of γ . Such behavior of $\eta(\mathcal{M}, \gamma)$ at $\mathcal{M} \in [0.1, 1]$ is a guideline for establishing the basic mechanism of acoustic wave generation in a compressible turbulent time-developing mixing layer, studied numerically in the next section.

III. DNS OF COMPRESSIBLE TIME-DEVELOPING MIXING LAYER

The simulations are performed to capture the essence – the basic mechanism – of the acoustic wave generation in shear flows by means of a compressible turbulent time-developing mixing layer. We solved the Navier-Stokes equations numerically using the optimized summation-by-parts dispersion relation preserving finite difference scheme of sixth-order accuracy in space and a third-order low-storage Runge-Kutta scheme in time [39, 40]. The convective Mach number of the time-developing shear layer between two (U_1 and U_2) anti-parallel streams of fluid with equal absolute values of velocities, $U_1 = -U_2 = \Delta U/2$, and constant density and sound speed, is defined by

$$M_c = \frac{\Delta U}{2c_s}. \quad (6)$$

The initial velocity profile is given as a hyperbolic tangent function for the mean streamwise velocity and shearwise and spanwise mean velocity components are set to zero (see Figure 3):

$$U(y) = \frac{\Delta U}{2} \tanh\left(\frac{y}{2\delta_\theta(0)}\right), \quad V = 0, \quad W = 0, \quad (7)$$

where $\delta_\theta(0)$ is the initial momentum thickness of shear layer. The momentum thickness of shear layer, $\delta_\theta(t)$, varies in time and represent s one of appropriate length scales used to describe the flow. The vorticity thickness, $\delta_\omega(t)$, is an

another widely used length scale. The definitions have the form:

$$\delta_\theta(t) = \frac{1}{\rho_0} \int_{-L_y/2}^{L_y/2} \bar{\rho} \left[\frac{1}{4} - \left(\frac{\bar{u}_1}{\Delta U} \right)^2 \right] dy; \quad \delta_\omega(t) = \frac{\Delta U}{|dU/dy|_{max}}; \quad Re_{\delta_\theta(t)} = \frac{\Delta U \delta_\theta(t)}{\nu}; \quad Re_{\delta_\omega(t)} = \frac{\Delta U \delta_\omega(t)}{\nu}. \quad (8)$$

Broadband disturbances are superimposed on the basic flow to trigger transition to turbulence in the flow [40]. The initial extent of the superimposed perturbations is limited in the shearwise direction to the initial shear layer thickness (the grey area on Figure 3). The turbulence develops in time leading to an increase of the shear layer thickness.

The numerical parameters of the numerical simulations presented are given in Table I. We performed simulations for the following convective Mach numbers $M_c = 0.3, 0.7$. The initial Reynolds numbers based on the momentum and vorticity thicknesses at the initial moment of time were chosen as $Re_{\delta_\theta(0)} = 800$ and $Re_{\delta_\omega(0)} = 3200$. The last column of the table represents the growth rate of the shear layer in the self-similar period of evolution in time when the linear growth rate is achieved.

Case	$(L_x \times L_y \times L_z)/\delta_\theta(0)$	$N_x \times N_y \times N_z$	L_x/L_z	M_c	$Re_{\delta_\theta(0)}$	Re_{δ_θ}	Re_{δ_ω}	$\dot{\delta}_\theta$
1	$100 \times 200 \times 50$	$1024 \times 1025 \times 512$	2.0	0.7	800	9256	37040	0.0047
2	$100 \times 200 \times 100$	$1024 \times 1025 \times 1024$	1.0	0.7	800	11256	43920	0.0062
3	$100 \times 200 \times 200$	$1024 \times 1025 \times 2048$	0.5	0.7	800	12593	47414	0.0072
4	$100 \times 200 \times 50$	$512 \times 1025 \times 256$	2.0	0.3	800	7230	27500	0.0081
5	$100 \times 200 \times 100$	$512 \times 1025 \times 512$	1.0	0.3	800	7472	27970	0.0106
6	$100 \times 200 \times 200$	$512 \times 1025 \times 1024$	0.5	0.3	800	6211	29736	0.0120

TABLE I: Simulation parameters: L_i and N_i ($i = x, y, z$) are domain lengths and number of grid points correspondingly. The simulations were performed for the convective Mach numbers $M_c = 0.3, 0.7$. Re_{δ_θ} and Re_ω are final Reynolds numbers based on the momentum and vorticity thicknesses respectively. $\dot{\delta}_\theta = d(\delta_\theta(t))/dt$ is the growth rate of shear layer within the self-similar period of evolution in time.

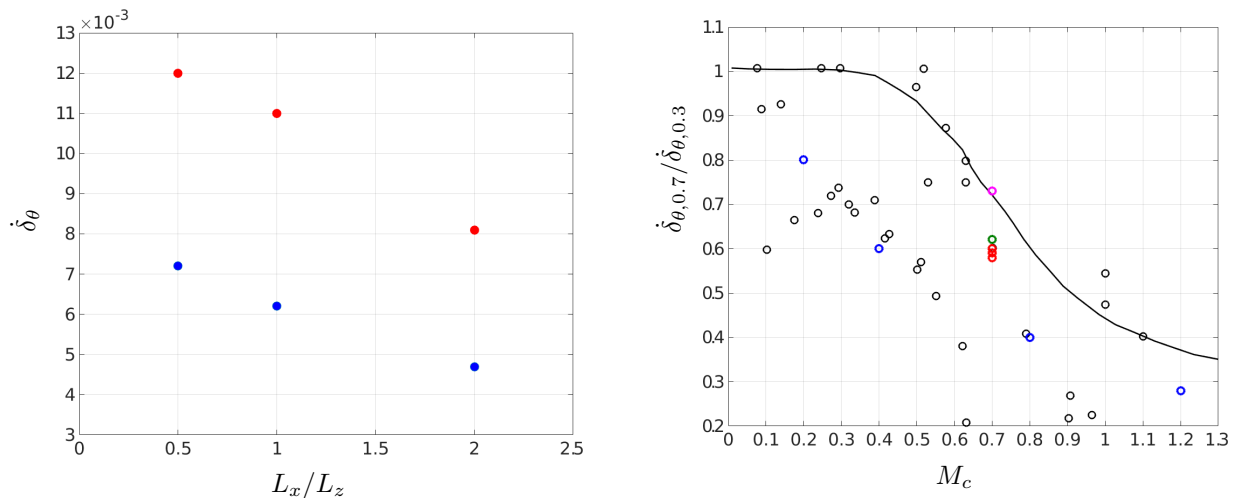


FIG. 4: Left plot: Growth rates vs. simulation box ratios for $M_c = 0.3, 0.7$, red and black points correspondingly; Right plot: Growth rate ratios from the different experimental and numerical studies of the flow in terms of convective Mach number. Black circles, see Pantano and Sarkar [39], Foysi and Sarkar [40], Matsuno and Lele [41] for references and details. The blue circles correspond to the recent results of Matsuno and Lele (2020) [41]. The red circles are from the present simulations for different L_x/L_z ratios. The green and magenta circles correspond to the cases A7 from Pantano and Sarkar, 2002 [39] and LES07 from Foysi and Sarkar, 2010 [40], correspondingly. The black solid line corresponds to the Langley experimental curve.

The growth rates vs. simulation box ratios (L_x/L_z) for $M_c = 0.3$ and 0.7 with red and black points, correspondingly are shown on left plot in Figure 4. As one can see, the increase of box ratio leads to the decrease of the growth rate

for both Mach numbers. The growth rate ratios ($\dot{\delta}_{\theta,0.7}/\dot{\delta}_{\theta,0.3}$) for different experimental and numerical studies are presented on the right plot in Figure 4. The blue filled circles correspond to the recent results for different Mach numbers by Matsuno and Lele (2020). The black filled circles represent different experimental and numerical results publishes in the literature (details for each points can be found in the literature, see, for example the papers by Pantano and Sarkar [39], Foyi and Sarkar [40], Matsuno and Lele [41] and references therein). As one can see the growth rate ratios of our simulations (red open circles) are in good agreement with those available in the literature. Here it is worth to note that for calculation of the growth rate ratios, we used the same simulation box ratios L_x/L_z for the both Mach numbers. As one can see, in the case of quasi-incompressible case, at $M_c = 0.3$, the increase of box ratio leads to the growth rate decrease that is clearly seen on the left plot in Figure 4. The mean profiles and RMS of streamwise velocity for aspect ratios corresponding to Cases 1-3 in self-similar period of flow development are presented in Figure 5. The turbulent stress tensor is defined as $R_{ij} = \rho u_i'' u_j'' / \bar{\rho}$, with Favre fluctuations [39, 40]. The collapse of Reynolds stresses and mean velocities is observed as it is expected in the self-similar period. As one can see from the figure, the peak values of the RMS of streamwise velocities decrease with increasing of the aspect ratios of the simulation boxes.

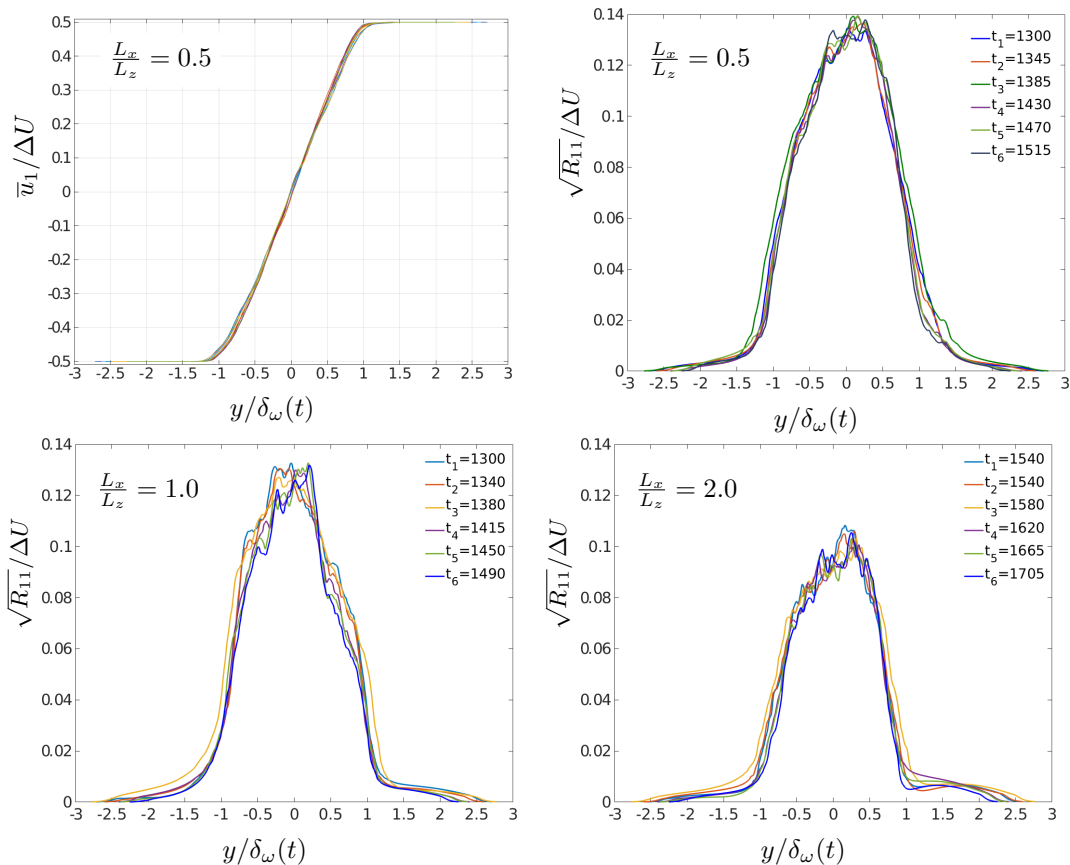


FIG. 5: Streamwise velocity profiles for $L_x/L_z = 0.5$ in the self-similar period of development of the flow; RMSs of streamwise velocity in self-similar period of development at multiple time samples are presented. From left to right: $L_x/L_z = 0.5$; $L_x/L_z = 1.0$, $L_x/L_z = 2.0$.

The aim of the first three cases of simulations is to show the main results of the work, to identify the origin of the acoustic wave output. The main difference between these cases is the different streamwise-spanwise aspect ratios (L_x/L_z) of the simulation boxes that define the characteristics of large scale eddies/harmonics of the turbulence. For instance, in Case 2 the mixing layer turbulence, in comparison with Case 1, contains a large scale harmonic with the wavelengths $\lambda_x = 100, \lambda_z = 100$. In Case 3, furthermore, the turbulence is even richer, additionally containing the harmonic with $\lambda_x = 100, \lambda_z = 200$ that is quite active in acoustic wave generation process. These different spectral contents of the turbulence in Cases 1-3 slightly influence the establishment of the self-similar state during the simulations, which can be seen in Figure 6, showing the momentum thicknesses, $\delta_\theta(\tilde{\tau})$, vs. the normalized time $\tilde{\tau} = t\Delta U/\delta_\theta(0)$. In the self-similar region ($\tilde{\tau} > 1300$), the mixing layer grows linearly with the growth rates depending on the aspect ratios of the simulation boxes: $\dot{\delta}_\theta(\tilde{\tau}) = 0.007, 0.006, 0.005$ for $L_x/L_z = 0.5, 1, 2$, respectively. It is clear

that the growth rate $\delta_\theta(\tilde{\tau})$ decreases with increasing aspect ratio.

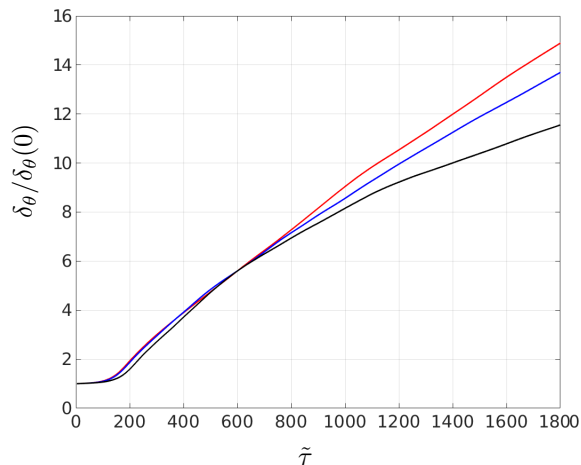


FIG. 6: Evolution in time of the momentum thickness normalized on the initial value, $\delta_\theta(\tilde{\tau})/\delta_\theta(0)$, for different aspect ratios of simulation boxes L_x/L_z : 0.5 (red line), 1.0 (blue line), and 2.0 (black line), from top to bottom.

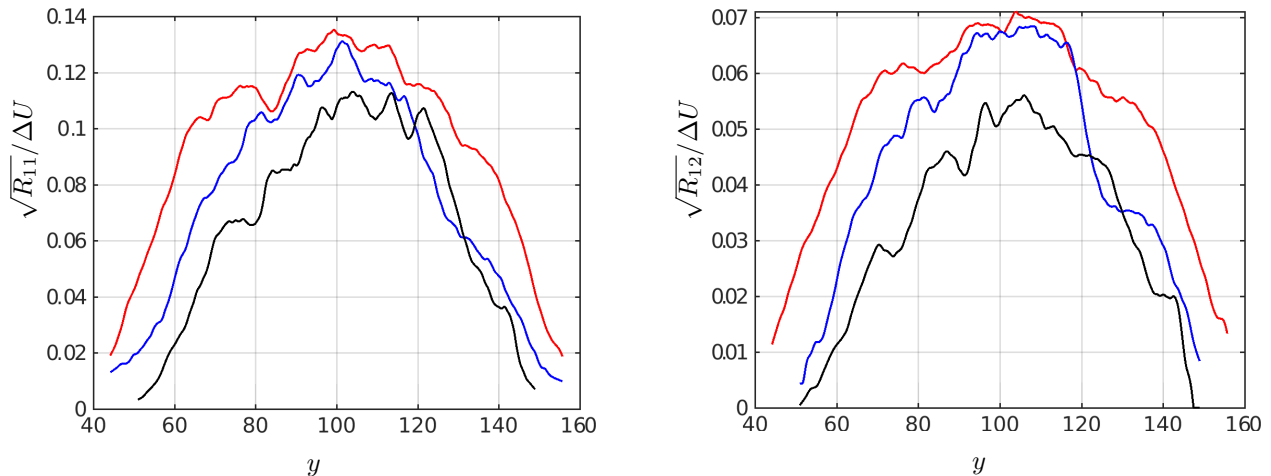


FIG. 7: Profiles of the RMS-velocity and shear stress for different aspect ratios of simulation boxes L_x/L_z : 0.5, 1, 2, dashed red, fine dashed blue and solid black lines correspondingly in the self-similar state at $\tilde{\tau} = 1600$.

Figure 7 shows the RMS of the streamwise velocity and shear stress for different aspect ratios of the boxes. These quantities are presented in a fixed moment of time (i.e., without averaging in time), therefore, they have not a very regular look. The figure shows significant influence of the box ratio on the turbulence intensity – it decreases with increase of L_x/L_z . Figure 8 shows the geometrical characteristics of the shear layer in the self-similar region, at $\tilde{\tau} \approx 1300$, for Case 1 ($M_c = 0.7$, right plot) and at $\tilde{\tau} \approx 930$, for Case 4 ($M_c = 0.3$, left plot). The central region (with constant shear rate) is more than 50% of the mixing layer total width. In addition, in this region, the shear rate substantially exceeds the rate in the rest of the layer. Therefore, it is natural that this region is dominant in the generation process of acoustic waves and, ultimately, in the formation of the near wave field.

According to the view presented in Sect II, the basic “elements” of the linear wave generation mechanism in constant shear flows are the Kelvin modes – the harmonics of the perturbations. Therefore, below we analyse the acoustic wave generation in terms of Kelvin modes in the central part of the shear layer.

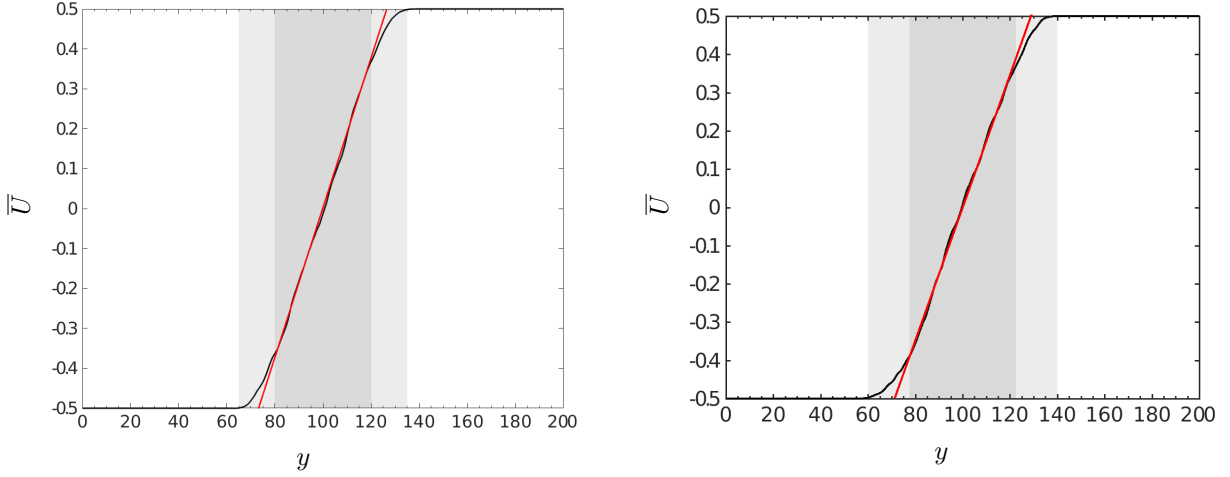


FIG. 8: Mean velocity profiles (the black line) in the self-similar period of the flow evolution for $M_c = 0.3$ (left plot) and $M_c = 0.7$ (right plot) are shown at $\tilde{\tau} \approx 930$ and $\tilde{\tau} \approx 1300$, correspondingly. The red line shows the maximum gradient of the mean velocity. The grey area represents the turbulent region of the flow. The dark grey area corresponds to the central/body region of the flow with linear mean velocity profile which matches to the red line. So, the red line inclination defines the shear rate, $A(\tilde{\tau})$, in the body region – the region of the acoustic wave mode generation. In the marginal, right and left white areas the near acoustic wave fields (generated in the central area and then emitted from the shear layer) are formed.

To grasp the essence of our view on the wave generation process and apply it to the compressible turbulent time-developing shear layer, one should understand the difference and define quantitative relation between M_c and \mathcal{M} . The former is determined only through general flow parameters, whereas the latter depends on the parameters of the central part of the shear layer and its perturbation harmonics as $\mathcal{M} = A/(k_x c_s) = A\lambda_x/2\pi c_s$, where λ_x is the streamwise wavelength of the harmonic and A is the shear rate. One can determine A from the inclination of the red lines in Figure 8: $A = \Delta U/\Delta y$. Similarly, two different nondimensional times connected to the wave harmonics, $\tau = c_s k_x t$ and to the shear layer, $\tilde{\tau} = t\Delta U/\delta_\theta(0)$ have been introduced. Taking Equation (6) into account, one gets the following relation between the Mach numbers:

$$\mathcal{M} = \frac{\Delta U \lambda_x}{2\pi c_s \Delta y} = \frac{M_c \lambda_x}{\pi \Delta y}. \quad (9)$$

From this equation we can get the following values of the mode-dependent Mach number \mathcal{M} for $M_c = 0.3, 0.7$ in the self-similar period of flow development, $\tilde{\tau} \approx 930, 1300$, correspondingly:

$$\mathcal{M}^{0.7} = \frac{0.7\lambda_x}{\pi 60} \quad \text{and} \quad \mathcal{M}^{0.3} = \frac{0.3\lambda_x}{\pi 50}. \quad (10)$$

We analyze the acoustic wave generation in the self-similar period where the growth rate of the momentum thickness remains constant, i.e., at $\tilde{\tau} > 1300$ (see Figure 6). Below we present and analyze the wave generation and dynamics specifically at $\tilde{\tau} \approx 1600$ for $M_c = 0.7$. At first, we calculate the mode-dependent Mach number for the first/largest streamwise harmonics with the wavelength equal to the box streamwise size, $\lambda_{x1} = L_x = 100$. From Equation (10), for $M_c = 0.7$, the mode-dependent Mach number for the first/largest streamwise harmonic can be calculated: $\mathcal{M}^{0.7}(\lambda_{x1}) \approx 0.372$. From the equation it follows that the mode-dependent Mach number decreases proportionally with λ_x . Therefore, for the second harmonic, $\lambda_{x2} = 50$, it is twice less, $\mathcal{M}^{0.7}(\lambda_{x2}) \approx 0.186$, etc. From the right plot in Figure 2 one can see that the wave generation is significant at $\mathcal{M}^{0.7} \approx 0.372$, but it is negligible at $\mathcal{M}^{0.7} \approx 0.186$: $\eta(\mathcal{M}^{0.7} \approx 0.372) \approx 0.235$, $\eta(\mathcal{M}^{0.7} \approx 0.186) \approx 0.0069$, i.e., $\eta(\mathcal{M}^{0.7} \approx 0.372)/\eta(\mathcal{M}^{0.7} \approx 0.186) \approx 34$. Thus, in the analyzed shear layer with $M_c = 0.7$ and considered simulation boxes with streamwise length $L_x = 100$, there occurs a substantial generation only for acoustic wave harmonics with the largest streamwise wavelength $\lambda_{x1} = 100$.

In similar way, the wave generation for $M_c = 0.3$ can be analyzed. From Equation (10) we have: $\mathcal{M}^{0.3}(\lambda_{x1}) \approx 0.191$. Consequently, the ratio between high and low Mach numbers for $\lambda_{x1} = 100$ is $\eta(\mathcal{M}^{0.7} \approx 0.372)/\eta(\mathcal{M}^{0.3} \approx 0.191) \approx 18$, i.e. the flow is, in fact, quasi-incompressible at $M_c = 0.3$.

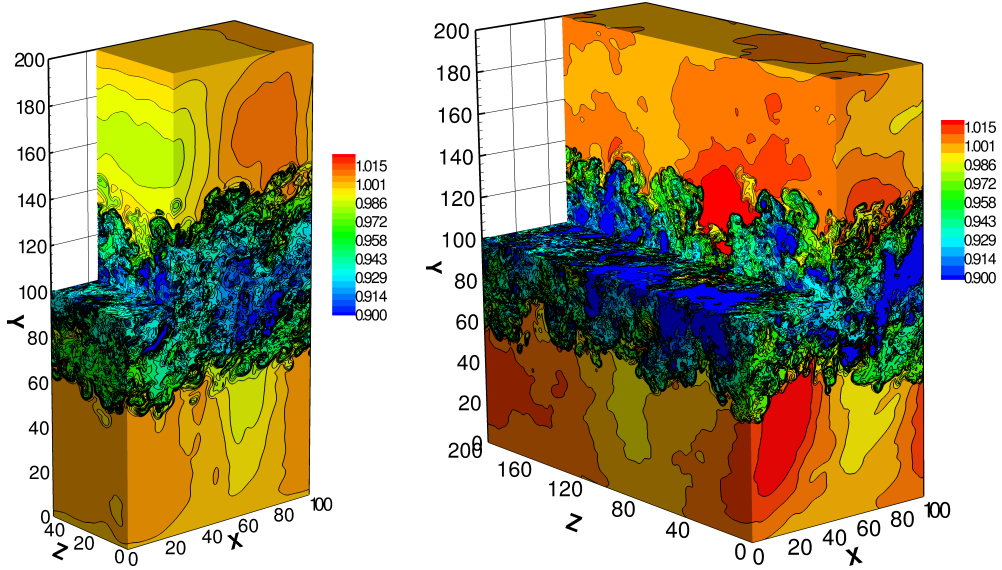


FIG. 9: 3D surfaces of the density field in the self-similar stage of the flow is shown in the turbulent mixing layer area and near far acoustic wave field areas. The left plot with the well pronounced 2D near field represents Case 1 ($L_x/L_z = 2$) and the right one with the well pronounced 3D near field shows Case 3 ($L_x/L_z = 0.5$). The near field configurations (iso-surfaces) for different aspect ratios are separately presented on Figures 11 and 13.

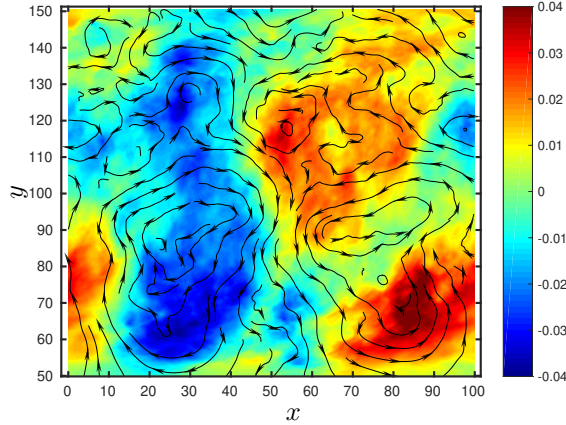


FIG. 10: xy -slice of spanwise averaged density and velocity streamtraces in the shear layer region ($50 < y < 150$) for Case 2 ($L_x/L_z = 1$).

For $\tilde{\tau} \approx 1600$, which corresponds to an instant within the self-similar development of the flow – the increase of the shear layer thickness occurs with a constant rate. The turbulence is expanding and “fills” the layer. Therefore, the linearly generated acoustic waves immediately appear outside the layer. Figure 9, that represents the simulation Case 1 with $L_x/L_z = 2$, shows that the shear layer area generally consists of 3D vortical turbulence, while the emitted acoustic field is mostly 2D. Obviously, the 3D turbulent field of the shear layer contains 2D components responsible for the generation of 2D acoustic waves. Spanwise averaging of the density and velocity perturbation fields, presented in Figure 10, reveals such 2D components in the mixing layer central region ($50 < y < 150$). As one can see, mainly the vortex component with maximum wavelength ($\lambda_x = 100$) is pronounced, although lower harmonics ($\lambda_x = 50, 25$) are also traced that weakly violate the regular patterns of the largest harmonic. From this ensemble of 2D vortex harmonics (for the considered convective Mach number, $Mc = 0.7$) the dominant contribution to the generation of acoustic waves (as it is calculated above) is given by the largest one.

According to Equation (3) the mode-dependent Mach number for 3D harmonics, \mathcal{M}^* , decreases with increase of γ . Consequently, the wave generation also decreases with increase of γ . In Case 1, for the harmonic with the largest streamwise wavelength, the minimal value of spanwise normalized wavenumber is $\gamma = \lambda_x/\lambda_z = L_x/L_z = 2$. The calculated efficacy of the wave generation for this 3D harmonic is $\eta(\lambda_x = 100, \lambda_z = 50) = 3.2 \cdot 10^{-7}$ which is negligible

compared to $\eta(\lambda_x = 100, \lambda_z = 0) = 0.32$. This explains the pronounced 2D nature of the acoustic wave density near field outside the shear layer. The 2D structure of this field is even more strongly pronounced in Figure 11 where the near field for two values of density, corresponding phases of compression ($\rho = 1.004$, red color) and rarefaction ($\rho = 0.996$, blue color) is presented. The left and right plots represent Case 1 and Case 2 correspondingly. The 2D structure of the near wave field is less established in Case 2 (there is an additional admixture of 3D wave harmonics), where the minimal value of spanwise normalized wavenumber is $\gamma = \lambda_x/\lambda_z = L_x/L_z = 1$.

For clarity we present one more Figure 12 for Case 1. It shows three iso-surfaces of the near density field. The left group of iso-surfaces of the blue color corresponds to three surfaces of the density in the rarefaction phase ($\rho = 0.992, 0.994, 0.996$) and the right group (red color) corresponds to three surfaces of the density in the compression phase ($\rho = 1.002, 1.004, 1.006$). Some visible irregularity of the right inner surfaces are traces of weak subsequent harmonics.

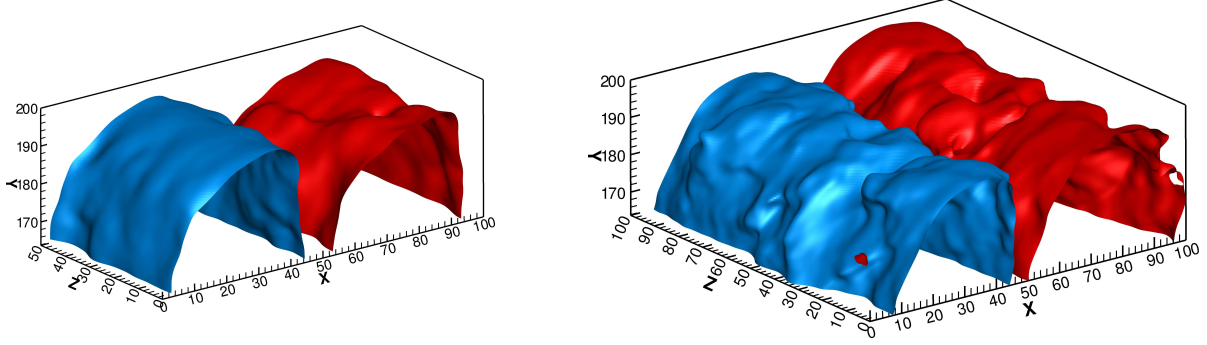


FIG. 11: Iso-surfaces of the near density fields with $\rho = 0.996$ (blue) and $\rho = 1.004$ (red). The left and right plots correspond to Case 1 and Case 2 correspondingly.

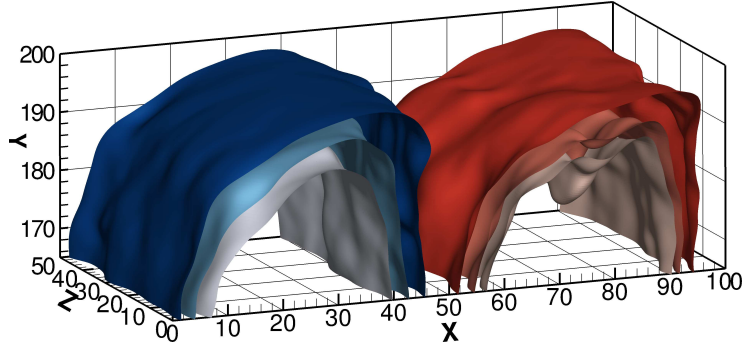


FIG. 12: Iso-surfaces of the near density fields with $\rho = 0.992, 0.994, 0.996$ (blue color group) and $\rho = 1.002, 1.004, 1.006$ (red color group) at $L_x/L_z = 2$.

The picture of the density field is fundamentally different in Case 3, where the lower minimal value of the spanwise normalized wavenumber for the harmonic with the largest streamwise wavelength is $\gamma = \lambda_x/\lambda_z = L_x/L_z = 100/200 = 0.5$. The calculated efficacy of the wave generation for this largest 3D harmonic is $\eta(\lambda_x = 100, \lambda_z = 200) = 0.22$ that is comparable to the efficacy of the related 2D harmonics $\eta(\lambda_x = 100, \lambda_z = 0) = 0.32$ (compare also the amplitudes of the black and red lines of the right column of Figure 1). Therefore the near density field represents a mix of these 2D and 3D harmonics. This complex picture is containing a significant 3D component in the near field and is shown in Figure 13, where (as in Figure 11) the near field of the density corresponding to phases of compression ($\rho = 1.004$, red color) and rarefaction ($\rho = 0.996$, blue color) is presented.

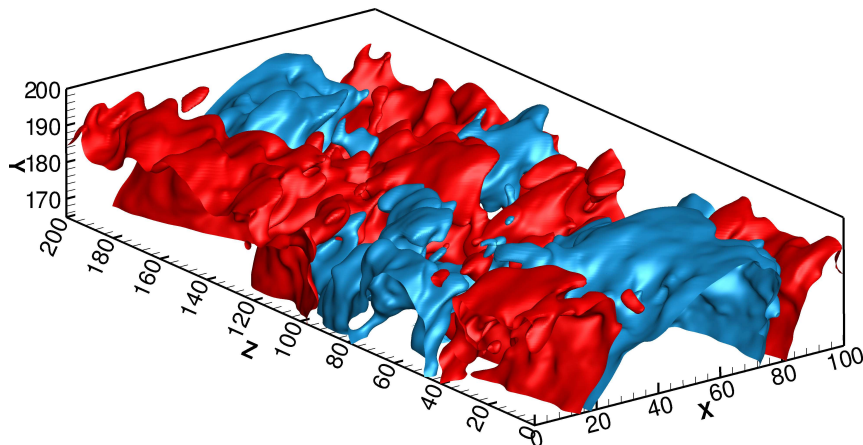


FIG. 13: Iso-surfaces of the near density fields with $\rho = 0.996$ (blue) and $\rho = 1.004$ (red) at $L_x/L_z = 0.5$.

Summarizing the results of DNS we can say that the near acoustic field exactly matches the characteristics of linearly generated acoustic waves in the central/body part of the shear layer due to the vortex–wave mode coupling induced by the shear flow non-normality as described in section II. The linear generation is substantial at $\mathcal{M} > 0.4$. This condition is satisfied by the harmonics of the considered shear layer (with $M_c = 0.7$ and $L_x = 100$) with the largest streamwise wavelength, $\lambda_x = 100$. The dominance of the largest streamwise harmonic is clearly seen from Figures 11 and 12. These figures correspond to Cases 1 and 2, for which the minimal values are $\gamma = 2$ and 1, respectively. For these cases the efficacy of 3D wave generation is small, $\eta \ll 1$ (see also Figure 1), therefore, the generated waves should be mostly 2D, which is clearly demonstrated by these figures. The very regular and smooth picture of the near wave field, shown in Figures 11 and 12, is easily explained from the abrupt and very regular character of the emergence of wave harmonics, according to which at the moment of the emergence, the shearwise velocity and density of the wave harmonic are zero, while the values of the streamwise and spanwise velocities are maximal (see item *(iv)* in section II). Due to this regularity, the wave harmonics generated at all subsequent moments are phase-correlated and interfere constructively. Therefore, ultimately, they give rise to a very regular and smooth near wave field presented in Figures 11 and 12. This time coherence of the generated acoustic waves is subsequently permanent in nature.

IV. SUMMARY AND DISCUSSIONS

The guideline of our efforts is the breakthrough within the hydrodynamic stability community in the comprehension of the shear flow non-normality and mathematical description of the non-normality induced phenomena. This trend formed in the hydrodynamic stability community in 1990s has been successfully adopted in atmospheric and astrophysical flow communities. A similar process is taking place in the fusion plasma community. Overall, the non-normality induced phenomena are inevitable in all – spectrally stable and unstable – shear flows as they essentially change the finite time period of the perturbation dynamics. The non-normality brings forth a new type of linear phenomenon – vortex–wave mode coupling that ensures the emergence of quite strong wave harmonics with very specific and regular initial characteristics. The key factor of the non-normality of the shear flow’s linear operators is demonstrated in our work on time-dependent shear layers. The main DNS result is the identification of the origin of the acoustic wave output, specifically, the demonstration of the dominance of the linear generation process of acoustic waves from the shear layer central part induced by the flow non-normality, on the acoustic wave near field emitted from the shear layer. This certainly justifies the importance of the shear flow linear operators non-normality and its consequence - non-modal dynamics of the perturbations - in the formation of acoustic wave output.

DNS and analysis performed for a specific shear flow give us an idea of the particular role of the wave-packets in the emission of acoustic waves from natural and engineering shear flows. One can consider a shear flow where not only the largest streamwise vortex harmonics are acoustically active, but also the subsequent shorter ones. If these vortex harmonics are coherent in space they will form a wave-packet. In this case, the spatial coherence of the wave-packet would be added to the temporal coherence of the acoustic wave generation mechanism described in section II. This would further amplify the generated acoustic waves while maintaining their regular/smooth pattern and eventually result in the formation of a regular/smooth near acoustic field which, in turn, evidently, transforms into the Mach waves. At a first glance it all looks like wave-packet generated acoustic waves. However, in fact, the waves are generated by the vortex harmonics due to the mechanism induced by the shear flow non-normality – the

wave-packet only collects the generated acoustic wave harmonics by constructive interference of the spatially and temporally coherent vortex harmonics of the wave-packet.

The configuration of the considered mixing layer is quite simple and permits to model the central part of the flow as a constant shear flow. In case any modal (exponentially growing) instability is absent – the only linear mechanism of acoustic wave generation is the vortex–wave coupling induced by the flow non-normality. However, an exponential growth of acoustic waves occurs in other kinds of engineering nonuniform flows with more complex velocity profiles, for instance in jet flows (see, e.g. [6] and references therein). Because of this, we consider it appropriate to present the influence on the modal instability of the non-normality of nonuniform flows when it occurs. *In general, the non-normality essentially changes the finite time period of any type of dynamical processes in such flows.* This equally applies to the linear transient phenomena in spectrally stable flows (e.g., transient growth of vortex mode perturbations, vortex–wave mode coupling) and to spectrally unstable flows, where exponentially growing “modal solutions” exist. From this the necessity follows to take the non-modal effects on the exponentially growing mode dynamics into account and not rely solely on its modal growth in order to properly describe and understand their real dynamics. Let us mention again, that this view about the importance of non-modal physics in the dynamics of exponentially growing modes is well comprehended by e.g. the astrophysical disk flow community [33, 34], too. Consequently, the modal approach of exponentially unstable modes of wave-packets in jet flows [6] can be misleading without involving the modifications of the spectrally unstable mode dynamics induced by the flow non-normality. The most justified way for nonuniform flows with complex velocity profiles is to adapt the generalized formulation of the non-modal approach [13, 15, 42, 43], that extends the modal stability theory to comprehensively account for all transient processes in different kind of shear flows, including the interaction between various modes and the mean flow, regardless of whether the modes are spectrally stable or not. In any case, further incorporation of phenomena induced by the shear flow non-normality in the aerodynamic acoustic wave generation process should be done in order to enhance the development of a refined theoretical framework to guide noise-control efforts.

Finally, we present an additional weighty argument justifying the importance of the linear vortex–wave coupling induced by the shear flow non-normality. The specificity of the linear acoustic wave generation mechanism substantiates the observations of two different sound generating mechanisms, i.e., omnidirectional and highly directional sound emission from fine-scale turbulence and large turbulence structures, respectively [44]. This is related to nonlinear and linear mechanisms. The direct influence of nonlinear (quadrupole) sources in the generation of acoustic waves in the considered case is negligible – to a greater degree acoustic waves are generated in the central/body part of the shear layer due to the vortex–wave mode linear coupling induced by the flow non-normality. It should be mentioned, however, that an indirect influence of the nonlinearity on the wave generation is significant – nonlinear phenomena take an active part in the formation of the turbulence spectrum, including the large scale coherent structures which are directly responsible for the generation of acoustic waves due to the above described linear mechanism. The main topological feature in spectral space of the linear mechanism of acoustic wave harmonics generation by vortex mode ones in constant shear flow is the following: the generation occurs when vortex mode harmonics cross the line of $k_y = 0$ in spectral space. Consequently, only up-shear tilted ($k_y/k_x > 0$) vortex harmonics have the generation potential and the linearly generated acoustic wave harmonics are only down-shear tilted ($k_y/k_x < 0$). Such a topology can not be reproduced by the linear source term representations of any classical formulation of an acoustic analogy [31]. The topological incompatibility of the linear source terms of the latter and the linear mechanism of wave generation induced by the flow non-normality is fundamental and, consequently, raises righteous questions about the validity of interpretations arising from applying of acoustic analogies to a shear flow systems.

V. ACKNOWLEDGMENT

This work was supported by the German Scientific Society (DFG) research grant No.FO 674/6-1. We gratefully acknowledge support with computing time from HPC facility at the university of Siegen.

-
- [1] C. K. W. Tam, Computational aeroacoustics: Issues and methods, *AIAA J.* **33**, 1788 (1995).
 - [2] J. Laufer and T.-C. Yen, Noise generation by a low-mach-number jet, *J. Fluid Mech.* **134**, 1 (1983).
 - [3] G. Crighton and P. Huerre, Shear-layer pressure fluctuations and superdirective acoustic sources, *J. Fluid Mech.* **220** (1990).
 - [4] L. Cheung and S. Lele, Linear and nonlinear processes in two-dimensional mixing layer dynamics and sound radiation, *J. Fluid. Mech.* **625**, 312 (2009).
 - [5] T. Colonius, S. K. Lele, and P. Moin, Sound generation in a mixing layer, *J. Fluid Mech.* **330**, 375 (1997).
 - [6] P. Jordan and T. Colonius, Wave Packets and Turbulent Jet Noise, *Annu. Rev. Fluid. Mech.* **45**, 173 (2013).

- [7] L. Gustavsson, Energy growth of three-dimensional disturbances in plane Poiseuille flow, *J. Fluid Mech.* **224**, 241 (1991).
- [8] K. Butler and B. Farrell, Three-dimensional optimal perturbations in viscous shear flow, *Phys. Fluids A* **4**, 1637 (1992).
- [9] L. Trefethen, A. Trefethen, S. Reddy, and T. Driscoll, Hydrodynamic stability without eigenvalues, *Science* **261**, 578 (1993).
- [10] S. Reddy and D. Henningson, Energy growth in viscous channel flows, *J. Fluid Mech.* **252**, 209 (1993).
- [11] S. Reddy, P. Schmid, and D. Henningson, Pseudospectra of the Orr-Sommerfeld operator, *SIAM J. Appl. Math.* **53**, 15 (1993).
- [12] P. Schmid and D. Henningson, *Stability and Transition in Shear Flows*, Applied Mathematical Sciences No. Bd. 142 (Springer, 2001).
- [13] P. Schmid, Nonmodal stability theory, *Annu. Rev. Fluid Mech.* **39**, 129 (2007).
- [14] L. Trefethen, Pseudospectra of linear operators, *SIAM Rev.* **39**, 383 (1997).
- [15] L. Trefethen and M. Embree, *Spectra And Pseudospectra: The Behavior of Nonnormal Matrices And Operators* (Princeton University Press, 2005).
- [16] D. Henningson, L. Gustavsson, and K. Breuer, Localized disturbances in parallel shear flows, *Applied Scientific Research* **53**, 51 (1994).
- [17] A. G. Tevzadze, Emission of magnetosonic waves by vortices in high shear flows, *Physics of Plasmas* **5**, 1557 (1998).
- [18] A. G. Tevzadze, G. D. Chagelishvili, J.-P. Zahn, R. G. Chanishvili, and J. G. Lominadze, On hydrodynamic shear turbulence in stratified Keplerian disks: Transient growth of small-scale 3D vortex mode perturbations, *Astron. Astrophys.* **407**, 779 (2003).
- [19] E. Heifetz and B. Farrell, Generalized stability of nongeostrophic baroclinic shear flow. Part I: Large Richardson number regime, *J. Atmos. Sci.* **60**, 2083 (2003).
- [20] J. Vanneste and I. Yavneh, Exponentially small inertia-gravity waves and the breakdown of quasigeostrophic balance, *J. Atmos. Sci.* **61**, 211 (2004).
- [21] M. V. Kalashnik, G. R. Mamatsashvili, G. D. Chagelishvili, and J. G. Lominadze, Linear dynamics of non-symmetric perturbations in geostrophic horizontal shear flows, *Q. J. R. Meteorol. Soc.* **132**, 505 (2006).
- [22] J. Vanneste, Asymptotics of a slow manifold, *SIAM J. Appl. Dyn. Syst.* **7**, 1163 (2008).
- [23] E. I. Ólafsdóttir, A. B. O. Daalhus, and J. Vanneste, Inertia-gravity-wave radiation by a sheared vortex, *J. Fluid Mech.* **596**, 169 (2008).
- [24] F. Lott, R. Plougonven, and J. Vanneste, Gravity waves generated by sheared potential-vorticity anomalies, *J. Atmos. Sci.* **67**, 157 (2010).
- [25] G. R. Mamatsashvili, V. S. Avsarkisov, G. D. Chagelishvili, R. G. Chanishvili, and M. V. Kalashnik, Transient dynamics of nonsymmetric perturbations versus symmetric instability in baroclinic zonal shear flows, *J. Atmos. Sci.* **67**, 2972 (2010).
- [26] G. Favraud and V. Pagneux, Acoustic-vorticity coupling in linear varying shear flows using the WKB method, *Proc. R. Soc. A* **469**, 20120708 (2013).
- [27] J. Vanneste, Balance and spontaneous wave generation in geophysical flows, *Annu. Rev. Fluid. Mech.* **45**, 147 (2013).
- [28] G. Chagelishvili, A. Tevzadze, G. Bodo, and S. Moiseev, Linear mechanism of wave emergence from vortices in smooth shear flows, *Phys. Rev. Lett.* **79**, 3178 (1997).
- [29] B. Farrell and P. Ioannou, Transient and asymptotic growth of two-dimensional perturbations in viscous compressible shear flow, *Phys. Fluids* **12**, 3021 (2000).
- [30] G. Favraud and V. Pagneux, Superadiabatic evolution of acoustic and vorticity perturbations in couette flow, *Phys. Rev. E* **89**, 033012 (2014).
- [31] J.-N. Hau, G. Chagelishvili, G. Khujadze, M. Oberlack, and A. Tevzadze, A comparative numerical analysis of linear and nonlinear aerodynamic sound generation by vortex disturbances in homentropic constant shear flows, *Physics of Fluids* **27**, 126101 (2015).
- [32] N. Bakas, Mechanism underlying transient growth of planar perturbations in unbounded compressible shear flow, *J. Fluid Mech.* **639**, 479 (2009).
- [33] J. Squire and A. Bhattacharjee, Nonmodal growth of the magnetorotational instability, *Physical Review Letters* **113**, 025006 (2014).
- [34] D. Gogichaishvili, G. Mamatsashvili, W. Horton, and G. Chagelishvili, Active modes and dynamical balances in mri turbulence of keplerian disks with a net vertical magnetic field, *The Astrophysical Journal* **866**, 134 (2018).
- [35] To note is that we focused on the acoustic wave linear generation due to the linear vortex-wave mode coupling induced by shear flow non-normality. However, generally there exists another linear mechanism of the wave generation, which is also induced by the flow non-normality but not through the vortex mode – this mechanism leads to the direct extraction of the flow energy by acoustic waves [45, 46]. The growth of the acoustic wave harmonics is algebraic (i.e., not exponential), therefore it needs time to achieve palpable values to make any contribution to the near acoustic wave field. This is not a case for the considered time-developing shear layer – acoustic wave harmonics don't have enough time to extract mean shear flow energy directly and amplify. Therefore, we can not observe this process in our simulations. In this connection, the acoustic wave linear generation due to the vortex-wave mode coupling in the paper is referred to as the only mechanism.
- [36] Z. Yoshida, Kinetic theory for non-hermitian dynamics of waves in shear flow, *Phys. Plasmas* **12**, 024503 (2005).
- [37] G. Chagelishvili, New linear mechanisms of acoustic wave generation in smooth shear flows (nonmodal study), in *Sound-Flow Interactions*, Lecture Notes in Physics, Vol. 586, edited by Y. Aurégan, V. Pagneux, J.-F. Pinton, and A. Maurel (Springer Berlin / Heidelberg, 2002) pp. 210–237.
- [38] A. G. Tevzadze, *Velocity shear induced phenomena in solar and astrophysical flows*, Ph.D. thesis, Katholieke Universiteit Leuven (2006).

- [39] C. Pantano and S. Sarkar, A study of compressibility effects in the high-speed turbulent shear layer using direct simulation, *Journal of Fluid Mechanics* **451**, 329 (2002).
- [40] H. Foyi and S. Sarkar, The compressible mixing layer: an LES study, *Theoretical and Computational Fluid Dynamics* **24**, 565 (2010).
- [41] K. V. Matsuno and S. K. Lele, Compressibility effects in high speed turbulent shear layers - revisited, *AIAA SciTechForum* , 1 (2020).
- [42] B. Farrell and P. Ioannou, Generalized stability theory part I: Autonomous operators, *J. Atmos. Sci.* **53**, 2025 (1996).
- [43] B. Farrell and P. Ioannou, Generalized stability theory part II: Non-autonomous operators, *J. Atmos. Sci.* **53**, 2041 (1996).
- [44] C. K. W. Tam, K. Viswanathan, K. K. Ahuja, and J. Panda, The sources of jet noise: experimental evidence, *J. Fluid Mech.* **615**, 253 (2008).
- [45] G. D. Chagelishvili, A. D. Rogava, and I. N. Segal, Hydrodynamic stability of compressible plane Couette flow, *Phys. Rev. Lett.* **50**, R4283 (1994).
- [46] G. D. Chagelishvili, G. R. Khujadze, J. Lominadze, and A. D. Rogava, Acoustic waves in unbounded shear flows, *Phys. Fluids* **9**, 1955 (1997).